Shedding light on the formation and stability of mesostructures in ternary "Ouzo" mixtures

Déborah Iglicki, Clément Goubault, Mouktar Nour Mahamoud, Soizic Chevance, Fabienne Gauffre

Shedding Light on the Formation and Stability of Mesostructures in Ternary "Ouzo" Mixtures

*Déborah Iglicki, Clément Goubault, Mouktar Nour Mahamoud, Soizic Chevance and Fabienne Gauffre**

Univ Rennes, CNRS, ISCR – UMR 6226, ScanMat - UAR 2025, F-35000 Rennes, France

deborah.iglicki@univ-rennes1.fr
clement.goubault@gmail.com
mouktar.nour@univ-rennes1.fr
soizic.chevance@univ-rennes1.fr
fabienne.gauffre@univ-rennes1.fr ; +33 (0)2.23.23.63.98

Abstract

Hypothesis: Ternary systems made of water, a water-miscible solvent, and hydrophobic solutes spontaneously produce metastable particles by the "Ouzo effect" and thermodynamically stable "Surfactant Free Micro Emulsions" (SFME). However, the use of different analyses has led to a variability in the criteria to determine the boundaries of the Ouzo domain. We hypothesized that this could be clarified by investigating the stability and the physical state of the particles.

Experiments: We investigate four systems using both solid and liquid solutes and two different solvents, and achieved a careful investigation of their phase diagrams, using DLS, Nanoparticle Tracking Analysis, NMR, Multiple Light Scattering, electrophoretic mobility, and fluorescence analysis.

Findings: Our results evidence that the transition from the monophasic to the Ouzo domains does not coincide with the cloudiness curve, and that compositions in the Ouzo domain can look fully transparent, in contrast to what is often considered. This transition is best determined by stability analysis. The cloudiness curve corresponds to the formation of particles with a large size dispersity. In the Ouzo domain, we observed an exchange of solute between the continuous phase and solute particles swollen with solvent. In addition, the particles are stabilized against coalescence by their high negative charge.

Keywords: Emulsion, Nanoprecipitation, Ouzo effect, Phase diagram, metastability

1.Introduction

The role of the "Ouzo effect" in the elaboration of anis-flavored alcoholic beverage has long been recognized [1–4]. This phenomenon, more generally known as "nanoprecipitation" in the context of galenic and pharmaceutical sciences, is also widely used to elaborate polymer, drug or dye particles in the industry [5–7]. More recently, it has been shown that Ouzo emulsions can also template the formation of capsules from polymers, proteins or nanoparticles [7–11]. The Ouzo emulsions/suspensions form in ternary systems consisting of two miscible solvents and a solute, this latter being highly miscible in one solvent but poorly in the other one. In most reported cases, the system contains water as one solvent, a polar water-miscible

solvent (acetone, ethanol…) and a hydrophobic solute, such as an oil or a polymer [12,13]. From a practical point of view, a fine emulsion is best obtained by a rapid mixing of water with the organic phase containing the solute [14]. The solvent shift causes the instantaneous nucleation of solute-rich droplets that grow, fed by free solute molecules, following a "nucleation-and-growth" mechanism [1]. This first stage occurs rapidly (< 1s) and stops when the solute concentration in the continuous phase has decreased down to its saturation limit. A second period of droplet growth (t ~1h) is often described, either via coalescence or Ostwald ripening [5,15–17]. Interestingly, after this stage, droplet growth can be very slow and the colloidal stability of the samples can last for weeks. The existence of a charge on the surface of the droplets seems to be the most likely hypothesis to explain such stability. However, the origin of this charge is still a matter of debate [14,18,19]. The final size of the droplets/particles ranges from ca 100 nm to a few microns, depending on the composition and preparation pathway.

One of the most attractive features of Ouzo emulsions is that very narrow size distributions can be obtained at specific compositions. In addition, the nucleation-and-growth mechanism is a spontaneous phenomenon allowing the "bottom up" generation of droplets/particles with almost no external energy [1,4]. This contrasts with conventional "top down" emulsification, where a high amount of energy is needed to fractionate and disperse one phase into the other.

In many cases, the formation of nanoparticles by nanoprecipitation/Ouzo effect is based on empirical experience and visual observation of cloudiness. However, a precise knowledge of the phase diagrams can greatly improve the quality of the size distribution and also enable to elaborate multicomponent particles [9,10]. The ternary phase diagrams of Ouzo systems generally show a biphasic domain, separated from the monophasic domain by the binodal curve [20]. The other important curve is the spinodal curve, that sets the system stability limit. The space enclosed in between the binodal and the spinodal curves corresponds to a metastable region. Note that the Ouzo domain is a sub-area of the metastable region, that it is not thermodynamically defined and depends on sample preparation conditions [12,14]. For instance, the boundary determined by step-by-step addition of water to the solute organic solution often differs from that obtained by addition of water in one shot [12]. Very interestingly, thermodynamically stable microemulsions may be observed in the monophasic (transparent) domain [21]. These have been called "surfactant free microemulsion (SFME)" [22] or "pre-Ouzo ultraflexible microemulsions" [9,23]. Their sizes vary from a few [24–26] to ca 100 [9,16] nanometers, which suggests that they might have a different origin.

Various techniques were used to investigate the structures formed in the Ouzo systems and determine the boundaries between the different domains. Among them Dynamic Light Scattering (DLS) is the most frequently reported, as it is a widespread technology that can measure the size of Brownian particles from a few nanometers to a few microns. Its main limitations are that it is not appropriate for cloudy samples (due to multiple light scattering) nor for polydisperse samples (for which it is difficult to obtain a proper distribution). Small angle X-Ray Scattering and Neutron Scattering (SAXS and SANS) also brought interesting insights but cannot be used routinely [2,3,24,26]. A few studies have taken advantage of NMR to probe the size of the aggregates and the possible exchange of solute between the continuous phase and the aggregates [27,28]. Finally, electron microscopy is frequently used to image the particles obtained when working with solid solutes, particularly polymers [12,13].

Until now, most authors have identified the limit of cloudiness with the boundary of the Ouzo domain. This originates from the fact that the concept of Ouzo emulsions was developed to explain the cloudiness of this beverage, but the reciprocal —all samples in Ouzo domain should be cloudy— is not

necessarily true. More generally, it is a common mistake to identify the binodal with the cloudiness curve as recently pointed out by Arce et al [20].

In our group, we have used the water/THF/BHT (THF = Tetrahydrofuran, BHT = butylated hydroxytoluene) to elaborate capsules with a nanoparticle shell [16,29]. The choice of this system was driven by the fact that BHT, generally present in commercial THF as a radical scavenger, is known to generate submicronic droplets [30,31]. In this system, we observed transparent samples containing droplets of ca 100 nm. These samples were classified as SFME as they did not seem to evolve with time [16]. Interestingly, this suggests that samples in the Ouzo domain might also look transparent since we did observe a size continuity between both domains.

With the aim to find an objective method to determine the boundaries of the Ouzo domain we investigated in details the model system water/THF/BHT using Dynamic Light Scattering (DLS), Nanoparticle Tracking Analysis (NTA), Static Multiple Light Scattering (SMLS), Nuclear Magnetic Resonance (NMR) and electrophoretic mobility. In particular, we consider stability (i.e. no evolution of droplet size) as a criterion to distinguish between the SFME (stable) and the Ouzo (slow droplets growth) domains. Three new systems: water/THF/α-tocopherol, water/DMSO/limonene and water/THF/BODIPY are also considered.

2. Material and methods

Materials. Tetrahydrofuran (THF, inhibitor-free, HPLC grade, ≥99.9%) was purchased from Sigma-Aldrich. Butylated hydroxytoluene (BHT) was purchased from Janssen. (*S*)-4-Isopropenyl-1-methyl cyclohexene (S-(–)-limonene, 96%) was purchased from Sigma–Aldrich. (±)−α−Tocopherol (Vitamin E or Vit E) in oil solution from BASF was graciously provided by AMI-ingredient. 4-Difluoro-8-(4-trimethylsilylethynylphenyl)-1,3,5,7-tetramethyl-2,6-diethyl-4-bora-3a,4a-diaza-s-indacene (BODIPY) was synthesized following a reported procedure [32]. Samples were made using MilliQ water (18.2 MΩ.cm).

Sample preparation and elaboration of the phase diagram. In all cases, samples were prepared by adding water to a solvent (THF or DMSO) containing the hydrophobic solute (BHT, limonene, α-Tocopherol or BODIPY) in one shot. The water is added promptly using a micropipette and the sample is vortexed about 10 s unless stated otherwise. For elaborating the phase diagrams, the samples were immediately visually inspected under the light of a telephone flash. The limpid and homogeneous solutions were classified in the monophasic phase. If we observed a light scattering and a cloudiness inside the homogeneous samples, we attributed them to the Ouzo domain. If we saw any precipitates in the samples, or any oil droplets at the top of the solutions, we placed them in the diphasic domain. Concerning the elaboration of the BODIPY phase diagram in THF and water, the samples were made as previously explained and they were observed under UV illumination at $\lambda_{excitation}$ = 365 nm. Then we took a photography of each series at the different solvent fraction. And we placed a spot of the same color as the sample from these photos in the phase diagram at the coordinates corresponding to the different mass fractions of BODIPY and solvent used.

Static Multiple Light Scattering (SMLS). A Static Multiple Light Scattering (SMLS) device (TurbiScan™ TOWER) from Formulaction (France) was used for monitoring the stability of the emulsions. The device measures Transmission (T, at 180°) or Backscattering (BS, at 45°) intensities over the sample height over time using a near infrared light source (λ = 880 nm) and two synchronous detectors that move

up and down along the sample. The samples were prepared in glass vials by adding water in one shot to the organic solution. For mixing, each sample was slowly turned over 3 times and monitored by the TurbiScan™ instrument and the TowerSoft software for 14 h. Results are provided as the relative transmission.

Nanoparticle Tracking Analysis (NTA). NTA was carried out using a Nanosight LM10 device (Malvern Panalytical). The sample was inserted into the cell of the device and illuminated by a laser beam (40 mW, $\lambda = 405$ nm). The light scattered by the droplets appears as individual spots and recorded by a CCD camera, operating at 30 frames per second, through a microscope. For each sample, measurements were achieved a few minutes after mixing and after 3 h. Each measurement consists of 3 acquisitions of 30 s. Thanks to the NANOSIGHT NTA 2.0 Analytical Software, the size of each object was then individually deduced from the analysis of its Brownian motion. Measurement are operated at 25°C and calculations of the hydrodynamic diameters were achieved taking the viscosity of the THF/water mixture at this temperature from values reported by Das *et al* [33].

Dynamic Light Scattering (DLS). DLS measurements were achieved using a Vascokin DLS device from Cordouan (France) equipped with a contactless remote optical head measuring the scattered intensity from a laser diode (638 nm) at an angle of 170°. The scattered signal was acquired continuously during the desired time (1 to 3 h). Then, short sequences (typically of 1.5 to 3 min) were used at the selected time points for analysis. The hydrodynamic diameter (Z-average) is calculated by the method of the cumulants. Measurement temperature (room temperature) was monitored and input as a parameter in the cumulant fit.

Electrophoretic mobility. Electrophoretic mobility was measured using a Malvern Nanosizer operating at 633 nm and equipped with a dip cell (ZEN1002). Measurements were achieved right after mixing and after 15 min. The reported values represent the mean and standard deviation of three independent sets of 100 measurements.

Nuclear Magnetic Resonance (NMR). All spectra were recorded using the PRISM core facility on a Bruker AVANCE NEO 500 MHz spectrometer equipped with a 5 mm TCI ^{1}H- ^{13}C- ^{15}N cryo-probe. ^{1}H spectra were recorded at 298 K using standard Bruker sequences. Different compositions of D_2O/ THF-*d8*/BHT were analyzed by ^{1}H NMR. Briefly, the desired volume of BHT stock solution prepared in THF-*d8* was diluted into the desired volume of THF-*d8*. Then D_2O was quickly added and the solution was mixed 30 s by vortexing. NMR experiment was performed immediately after vortexing. The solution was then placed in a 5 mm NMR tube into which a coaxial tube was sometimes inserted but not systematically. This coaxial tube contained 200 µM of TSP (Trimethylsilyl)propionic-2,2,3,3-d_4 acid sodium salt) was used as external reference for calibration of the spectra and relative integration of the BHT signals. 2D ^{1}H NOESY experiments were carried out using the standard Bruker noesygpph sequence and the following acquisition parameters: mixing time of 500 ms, TD 4k x 128 points, 8 scans. This mixing time was long enough to detect chemical exchange. We used the freeware EXSYcalc (Mestrelab Research, https://mestrelab.com/software/freeware/) to estimate the kinetics constants k_1 and k_{-1} after integration of the off-diagonal cross-peaks. Self-diffusion measurements (DOSY experiments) [33] were carried out using a 2D Stimulated Echo experiment using bipolar gradients pulse sequence (***stebpgp1s***), with a diffusion delay (d20) of 350 ms and a gradient duration (p30) of 3 s. The diffusion dimension was processed with the 2D DOSY processing Topspin software (logarithmic scale).

3. Results and discussion

System water/THF/BHT. All samples in this study were prepared by addition of water to the organic solution in one shot, and no surfactant was used to stabilize the droplets. We first built a phase diagram water/THF/BHT by visual observations (see Figure SI-1 for a full diagram and Figure 1a for a zoom on the area of interest). We adopted the representation proposed by Vitale and Katz [1] where the mass fractions of solute and solvent are represented as horizontal and vertical axis respectively. The mass fraction of water is $\Phi_{Wat} = 1- (\Phi_{THF} + \Phi_{BHT})$. Since the region of interest is located at very small mass fractions of BHT, the corresponding axis is represented on a Log scale.

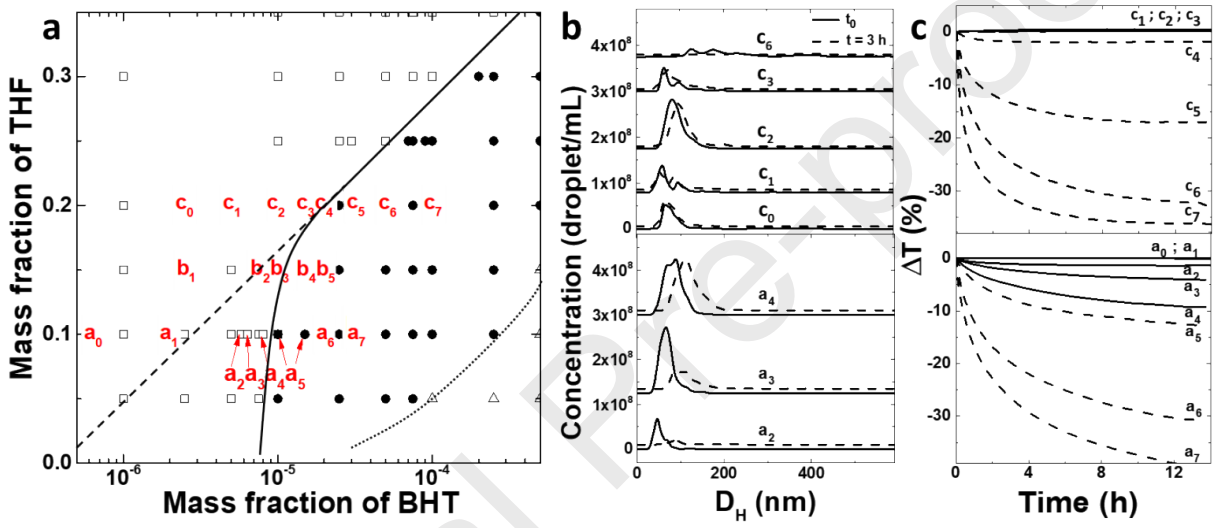

Figure 1: (a) Phase diagram water/THF/BHT determined by visual observation and focused on the area of interest: (□) limpid samples; (●) cloudy samples; (Δ) biphasic samples. (——) cloudiness curve, (- - -) linear extrapolation of the cloudiness curve, (.....) boundary between cloudy and macroscopically biphasic samples. (b) Size distribution measured using NTA at time 0 (——) and 3 hrs (- - -) for the compositions a_2-a_4 and c_0-c_6 as indicated on graph a. (c) SMLS stability analysis: relative transmission measured at mid-height of the samples. Full line (——): limpid samples; dashed line (- - -): cloudy samples

Sample	Mass fraction of BHT	Mass fraction of THF	D_H at t_0 (nm)	D_H at t_{3h} (nm)
$\mathbf{a_0}$	6×10^{-7}	0.1	69.9 ± 4.3	155.8 ± 2.8
$\mathbf{a_1}$	2×10^{-6}		62.4 ± 4.5	163.9 ± 5.1
$\mathbf{a_2}$	5.8×10^{-6}		64.4 ± 3.9	125.8 ± 2.1
$\mathbf{a_3}$	6.35×10^{-6}		70.8 ± 0.8	113.3 ± 1.4
$\mathbf{a_4}$	8×10^{-6}		67.4 ± 2.0	120.4 ± 12.2
$\mathbf{a_5}$	$1 \times 10^{-5} – 1.5 \times 10^{-5}$		121.7 ± 3.6	198.2 ± 7.9
$\mathbf{a_6}$	2×10^{-5}		141.9 ± 1.4	248.1 ± 6.5
$\mathbf{a_7}$	3×10^{-5}		-	-
$\mathbf{b_1}$	2.5×10^{-6}	0.15	-	-
$\mathbf{b_2}$	7.4×10^{-6}		-	-
$\mathbf{b_3}$	1×10^{-5}		-	-
$\mathbf{b_4}$	1.6×10^{-5}		-	-
$\mathbf{b_5}$	2×10^{-5}		-	-
$\mathbf{c_0}$	2.5×10^{-6}	0.2	85.3 ± 2.1	92.5 ± 5.9
$\mathbf{c_1}$	5×10^{-6}		87.5 ± 2.7	89.9 ± 8.4
$\mathbf{c_2}$	1×10^{-5}		93.5 ± 0.6	107.0 ± 2.1
$\mathbf{c_3}$	1.5×10^{-5}		95.2 ± 4.7	98.7 ± 1.5
$\mathbf{c_4}$	2×10^{-5}		69.9 ± 4.3	156.6 ± 3.0
$\mathbf{c_5}$	3×10^{-5}		-	-
$\mathbf{c_6}$	5×10^{-5}		231.9 ± 13.8	404.6 ± 28.6
$\mathbf{c_7}$	1×10^{-4}		-	-

Table 1: Composition of the samples of series a_n-c_n in the water/THF/BHT system, and mean hydrodynamic diameter of the distribution (D_H), as obtained by NTA at t=0 and t=3 h.

All samples were observed typically between 10 to 30 min after preparation. The full line represents the onset of cloudiness. At low THF fraction, the clouding is very subtle and difficult to detect by naked eyes. In this case, we used a cell phone light to shine the samples. At $\Phi_{THF} > 0.2$, the transition from transparent to cloudy compositions is more obvious and could be detected without a light. At high BHT concentrations, the samples rapidly form a thin turbid top layer, rich in oil (open triangles). We consider this limit (dotted line) as the spinodal line. The prediction of the binodal curves using semi-empirical methods to calculate the liquid-liquid equilibrium generally yield a straight line in the semi-Log representation [13]. Our own calculations of the binodal curve using COSMO-RS (Figure SI-1) also provide an almost straight line, however slightly shifted toward larger BHT mass fractions compared to the experimental data. Therefore, we assume that the linear portion of the cloudiness curve observed in the top part of the diagram is a good approximation of the binodal. The experimental curve clearly deviates from this expected linear behavior at mass fractions of THF lower than 0.2. In the following we investigate more specifically the samples series a_n, b_n and c_n as represented in Figure 1a (see Table 1 for compositions).

The composition line $\Phi_{THF} = 0.2$ (samples c_n) was selected for a first series of investigation because the location of the binodal curve is unambiguous. Samples of compositions ranging from $\Phi_{BHT} = 2.5\ 10^{-6}$ to $5\ 10^{-5}$ (c_0-c_6,) were analyzed using NTA ca 5 min after sample preparation, and also after 3 h to assess

sample stability (Figure 1b). It is obvious that samples c_0-c_3, that look transparent, contain in fact particles of diameter in the range 60-80 nm and show no significant evolution within 3 hours. Beyond the cloudiness curve ($c_{5\text{-}7}$), the samples become more polydisperse and exhibit larger sizes (> 100 nm) that exceed the limitation of the NTA (1µm) after 3 hours. An example of this behavior is sample c_6, shown in Figure 1b. These samples were also examined using DLS (Figure SI-2). For the most diluted samples (c_0-c_2), the scattered intensity is extremely low and a proper fit of the correlograms is prevented by the presence of a few very large particles (> 1µm). Figure SI-3 shows the effect of such large particles on the correlogram of composition c_1, together with the visual observation of the corresponding scattering spots using NTA. In contrast, sample c_3-c_6 could be analyzed. For compositions c_3 and beyond, we could achieve DLS analysis. Figure SI-2b shows the intensity-weighted size histogram for samples c_3 and c_6 shortly after mixing and after one hour. As expected, the mean size measured by DLS (225.6 ± 9.0 nm and 352.7 ± 11.4 nm for samples c_3 and c_6 at t= 0 respectively) is larger than those measured by NTA (95.2 ± 4.7 nm and 231.9 ± 13.8 nm respectively). In addition, the results confirm that c_3 does not evolve with time whereas the mean particle size increases over one hour for c_6.

It is important to note that the Ouzo systems investigated in the literature are often stabilized by the addition of surfactant to prevent coalescence [7,13]. Here, in the contrary, we assumed that monitoring the stability of the samples should be a method of choice to determine accurately the binodal curve. To this aim we used SMLS. The principle is to monitor the optical features (transmission and/or backscattering) during time and over the whole height of the sample. Coalescence or ripening is generally characterized by a similar evolution of the optical signal over the whole height of the sample, whereas sedimentation or creaming cause an uneven vertical optical signal. As an example, Figure SI-4 shows the time variation of the transmission (in relative values) for two samples on each side of the binodal curve: c_3, fully transparent and c_5, slightly cloudy. The transmission is measured all along the height of the vial. The kinetic behaviors of these two samples are strikingly different: sample c_3 remains stable over the 14 h of monitoring, whereas the transmission of sample c_5 clearly decreases with time, over the whole sample height. Very interestingly, the evolution of the sample reaches a stop after a few hours, but no sign of creaming or sedimentation was observed. This suggests that the mechanism(s) responsible for the growth of the droplets/particles is (are) hindered at some point. One hypothesis is that molecules (either free or under the form of very small aggregates) serving as a reservoir for the droplets are consumed [35]. Alternatively, the coalescence of droplets can come to a halt when their surface is efficiently covered by stabilizers [16]. The stability of samples c_1-c_7 was investigated, and the time evolution of the transmission measured at mid-height is reported Figure 1c. Consistently with the previous results, compositions c_1-c_3 are stable over the period of time considered, whereas c_5-c_7 show a significant diminution of their transmittance. Thus, SMLS analysis shows a clear transition in the colloidal stability of the samples. NTA and DLS measurement operated at different times confirm the stability behavior of the samples but are less convenient to use in this respect.

Encouraged by these results, we monitored the stability of samples along the composition lines Φ_{THF}=0.1 (samples a_1-a_7, Figure 1c) and Φ_{THF}=0.15 (samples b_1-b_5, Figure SI-5). Samples a_0 and a_1 are stable, whereas samples a_2-a_7 all evolve with time, with faster kinetics as BHT concentration increases. Similarly, compositions b_1-b_2 are stable, and b_3-b_5 unstable. Very interestingly, the samples a_2-a_4 and b_3 look fully transparent, but are in fact unstable. This confirms the fact that the visual determination of the binodal line is not an efficient method. On the other hand, the transition between stable and unstable compositions is consistent with the extrapolated straight-line in Figure 1a, for both series a_n and b_n. We further analyzed compositions in the area in-between the cloudiness curve and the extrapolated dashed line (a_2-a_4). Figure 1b

shows their size distribution at initial time and after 3 hours. All three samples clearly contain a distribution of particles growing in size over time, which confirms that these compositions are in fact metastable. Note that because the Ouzo effect is considered as a spontaneous emulsification, some authors suggested it requires no mixing and mixing modes should have no effect on the final size distribution. However, this is not true. The nucleation conditions in the Ouzo domain are sensitive to mixing conditions [14]. A rapid mixing rate (compared to nucleation rate) favors homogeneous nucleation. Therefore, we found it necessary to check if habits of different operators regarding mixing could influence our results, and found that it was not the case (see Supporting Information, Figure SI-6).

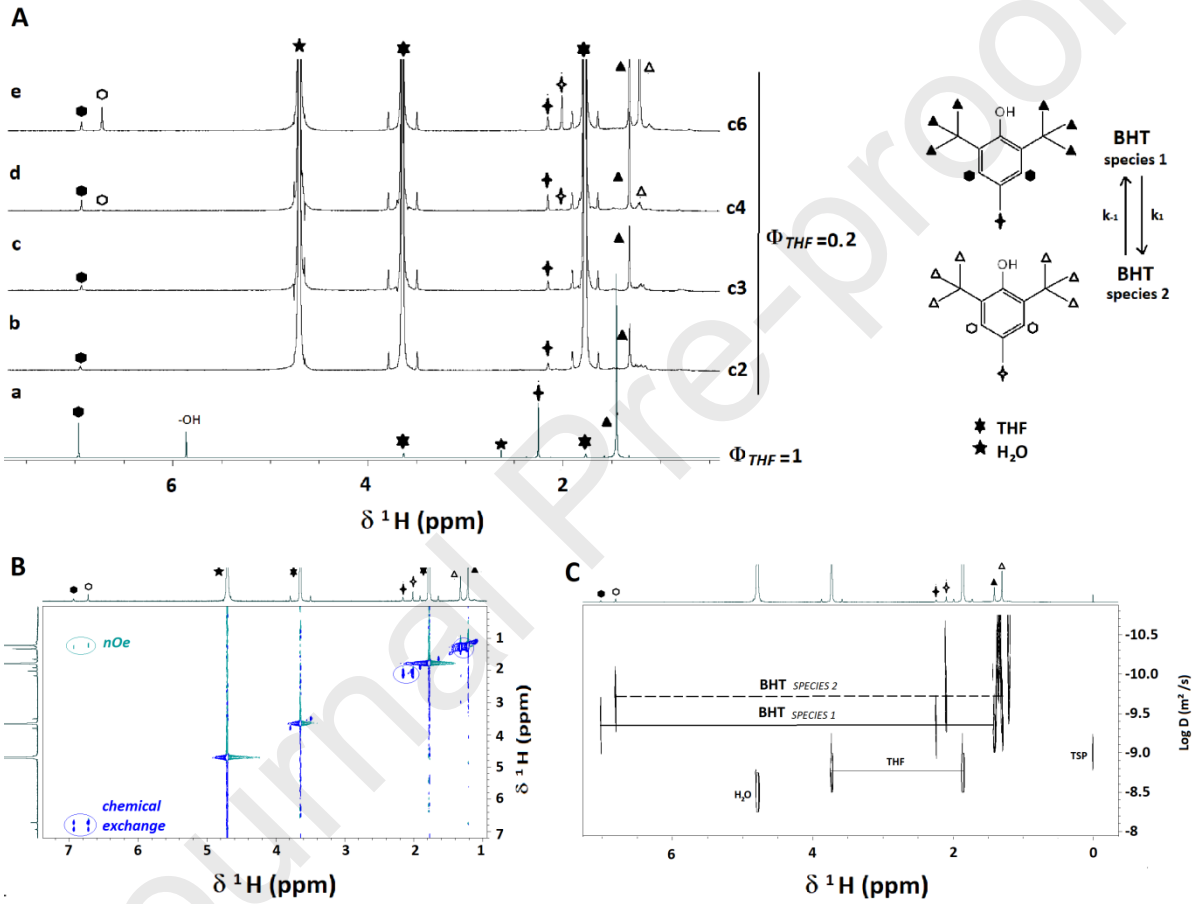

Figure 2: (A) 1D ^{1}H NMR spectra of BHT (a) solubilized in THF-d8 and (b-e) for samples along the composition line Φ_{THFd8} = 0.2 (c_2: $\Phi_{BHT} = 10^{-5}$; c_3: $\Phi_{BHT} = 1.5\ 10^{-5}$; c_4: $\Phi_{BHT} = 3\ 10^{-5}$; c_6: $\Phi_{BHT} = 5\ 10^{-5}$). The two sets of BHT proton resonances are identified by full and open symbols (▲/△, ♦/◊ and ●/○) as indicated on scheme. Solvent peaks are identified by filled stars: H_2O (★) and THF (✸). (B) 2D ^{1}H NOESY and (C) pseudo 2D ^{1}H DOSY NMR spectra of sample c_6.

In order to follow the transition from the monophasic to the Ouzo domain in more details, especially in terms of both BHT environment and mobility, we recorded the 1D ^{1}H NMR spectra of samples c_2-c_3 (SFME domain), c_4 (near the binodal) and c_6 (Ouzo domain). These spectra are presented in Figure 2A together with that of BHT solubilized in deuterated THF-d8. We can observe in spectra b-c a single set of

BHT signals for the compositions c_2 and c_3 (SFME domain). In addition, the chemical shifts of the methyl protons (▲) are significantly moved toward high field. These observations are consistent with BHT mainly dissolved in the continuous phase made of water/THF, and possibly in rapid exchange with SFME droplets. In contrast, the compositions c_4 and c_6 show two sets of signals (full and empty symbols, spectra d-e), revealing that the BHT is distributed between two different environments, most probably the dispersed and continuous phase, with slow exchange at the chemical shift time scale. This strongly suggests that the droplets that appear past the binodal have a different composition from that in the SFME. In a previous study of the water/ethanol/*trans*-anethol system, a similar behavior was found, and the systematic deshielding effect for the ^{1}H resonances of form 1 compared to form 2, was attributed to its more hydrophilic environment [35]. Moreover, the integration of the signals clearly shows that the proportion of BHT in this environment increases with the total amount of BHT: it represents > 60% of the BHT for the c_6 sample. To confirm the origin of these two sets of signals, we recorded the 2D ^{1}H NOESY (Nuclear Overhauser Effect SpectroscopY) spectrum of the sample c_6 (Figure 2B). This powerful experiment evidences, i) spatial correlations (nOes, distance < 5 Å) between two different protons (the green off-diagonal cross peaks in the Figure 5a) and ii) the presence of two species in chemical exchange (the blue off-diagonal cross peaks) [34,36,37]. This latter observation confirms the presence of two liquid BHT species in exchange, one in the continuous phase and the other in the dispersed phase. The exchange constant kinetics were estimated at k_1 and k_{-1} at 0.23 s^{-1} and 0.16 s^{-1} respectively [38]. To our knowledge, it is the first time that this exchange dimension between the continuous and dispersed phases is so clearly demonstrated. Then, we recorded DOSY spectra that allow us to discriminate the chemical species contained in a mixture in solution based on their self-diffusion coefficient. As shown in Figure 2C, the two BHT species coexisting in solution for sample c_6 do not have the same self-diffusion coefficient. The BHT contained in the continuous phase diffuses faster (~ 5 10^{-10} $m^2.s^{-1}$) than the BHT in the droplets of the dispersed phase (~ 2 10^{-10} $m^2.s^{-1}$). We can explain this result by a significantly higher viscosity in the dispersed phase compared to the continuous phase, due to the high BHT concentration within the droplets. The NMR analysis of the sample a_6 (Figure SI-7) yields similar conclusions as for the sample of composition c_6 presented above: two liquid BHT species coexist in solution and exhibit different diffusion coefficient, ~ 6.6 10^{-10} $m^2.s^{-1}$ and ~ 1.6 10^{-10} $m^2.s^{-1}$, corresponding respectively to the BHT in the continuous and dispersed phases. Note that the viscosity of the water/THF mixtures [33] is significantly lower for the composition a_6 (10% THF, η= 1.2 cP) compared to composition c_6 (20% THF, η= 1.5 cP), consistently with the higher diffusivity of the dissolved BHT in sample a_6. The predominant species is the BHT in the dispersed phase and represent ~75% of the total BHT. Unfortunately, despite the use of a more sensitive cryo-probe, the analysis of samples with lower BHT concentration was not possible.

As mentioned earlier, the presence of an electrostatic charge that inhibits coalescence is the most probable explanation for the slow evolution of Ouzo droplets over the long term. Therefore, we examined the electrophoretic mobility of the aggregates along the composition lines Φ_{THF}=0.1 and Φ_{THF}=0.2 (Figure 3). The mass fractions of BHT were normalized by their value at the binodal curve (dashed curve in Figure 1a), respectively Φ^*_{BHT}= 3.5 10^{-6} and Φ^*_{BHT}= 2 10^{-5}. It is striking that for both curves, the electrophoretic mobility is negative and reaches a minimum at the transition from the SFME to the metastable domains. Since the pH of these mixtures (pH=7 ± 0.5 and 6.5 ± 0.5 for Φ_{THF}=0.1 and 0.2 respectively) were relatively constant when varying the amount of BHT, this cannot be attributed to a change of concentration in OH^-. The strongly negative values (close to -80 mV in terms of zeta potential) reached for Φ_{THF}=0.1 explains the very slow evolution of compositions a_2-a_6 that was revealed by SMLS (Figure 1c). It has long been known that the

hydrophobic interfaces in water often carry a negative charge. Several hypotheses were proposed to explain this phenomenon, including the interfacial adsorption of endogenous negative ions such as water carbonates or hydroxides, or the presence of ionizable impurities [18,39]. Alternatively, some theoretical works assume that the surface charges from asymmetric charge density of water molecules in the vicinity of the interface [40]. Interestingly the coalescence of electrostatically repelling droplets can even lead to size focusing [17]. At the present time, we do not have a clear interpretation for the increase of surface charge close to the binodal. This could indicate a change in the droplet structure, with a sharper interface after the binodal than in the SFME.

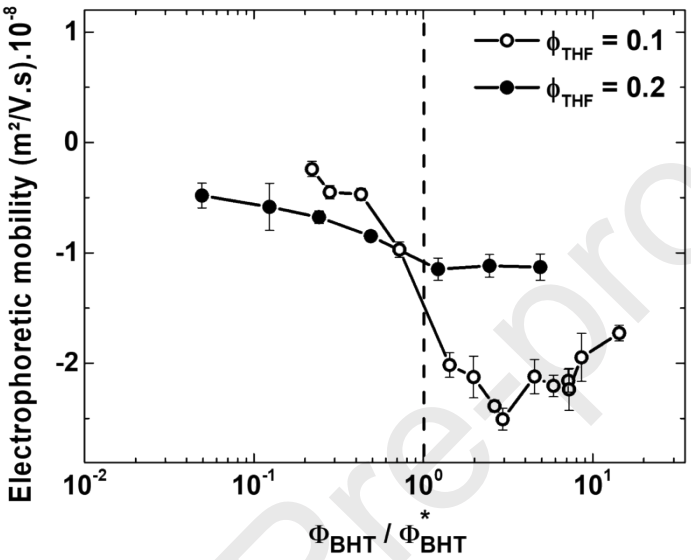

Figure 3: Electrophoretic mobility in function of the normalized concentration in BHT, for two compositions of THF (○: Φ_{THF}= 0.1 and ●: Φ_{THF}= 0.2). Φ_{BHT}^{*} represents the BHT mass fraction at the binodal. Error bars represent the standard deviation of 3 measurements.

At this point, we have confirmed that a simple visual observation is not appropriate to determine the location of the binodal in the water/THF/BHT system at low solute concentrations. Monitoring the evolution of the sample through light scattering techniques such as SMLS, but also NTA or DLS enables to find the expected linear shape of the binodal curve in the standard semi-Log representation. In order to generalize these findings, we decided to investigate new systems.

Investigation of systems with an oil as solute. We considered the systems water/THF/α-tocopherol and water/DMSO/limonene. Both limonene and α-tocopherol (vitamin E) are oils. The phase diagrams were first built by visual classification of the samples between limpid, cloudy and biphasic samples. As previously, the cloudiness curve deviates from the binodal at low solvent fractions (Figure 4). SMLS analysis was performed for compositions of interest (Figure SI-8). For the system water/DMSO/limonene, the stability analysis confirms that the binodal curve corresponds to the straight line extrapolated from the high concentrations. Indeed, compositions above this curve are stable, whereas compositions below this curve evolve with time. In the case of water/THF/α-tocopherol, the variations of transmittance for samples around the binodal curve are too small to properly identify the transition. This is due to the fact that the mass fraction of α-tocopherol at the binodal is below 10^{-6}, for the corresponding line. NTA analysis was also performed, and for each line, the mean hydrodynamic diameter is plotted as a function of the solute mass fraction normalized by the mass fraction at the cloudiness curve (full line, Figure 4). This representation

clearly evidences, for all three systems, a sudden increase (typically by a factor 2) in the mean size of the droplets at the cloudiness curve. In contrast, the size remains almost constant over two decades of mass fractions below this curve. Beyond this limit, the size becomes rapidly too large and/or the distribution too wide to be determined by NTA. Interestingly, this result indicates that the cloudiness curve is not a simple limit of detection but has a physical meaning. Our understanding of this boundary is that on its left side exists a transparent Ouzo domain consisting of small droplets (typically ≤ 100nm) with low dispersity, and on its right side a cloudy Ouzo domain with large and/or polydisperse droplets. At this point, it is interesting to note that there is a size continuity between the SFME and Ouzo domains. A possible explanation is that SFME aggregates exist in the Ouzo domain close to the boundary, as a supersaturated situation. However, the Ouzo domain is ultimately bound to form two separate phases. Therefore, these aggregates will evolve slowly to form Ouzo droplets, and ultimately a separate phase.

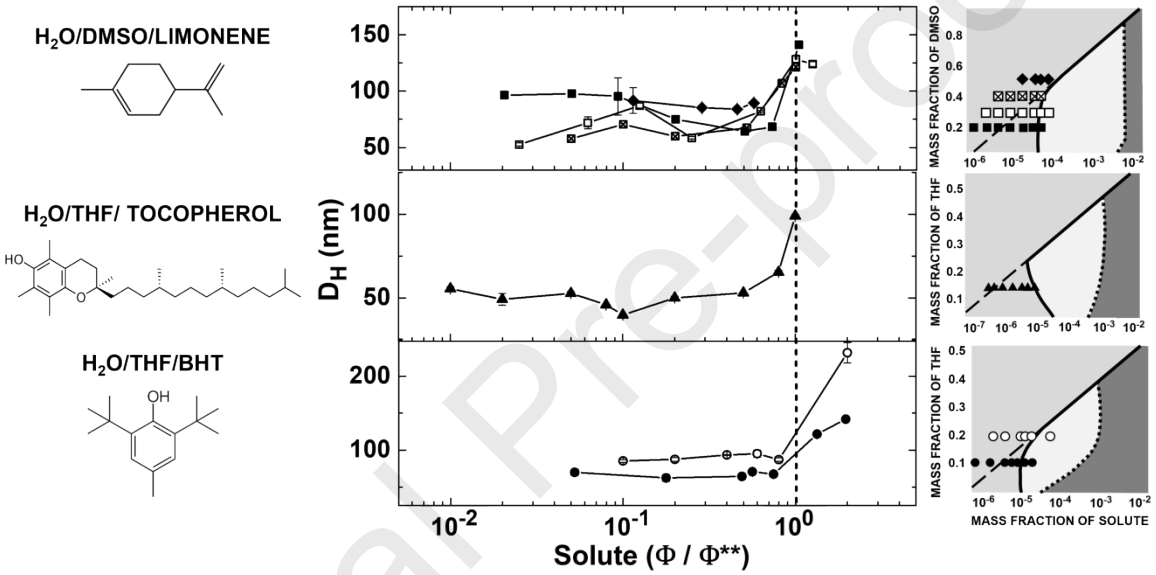

*Figure 4: Molecular formula of the solutes; mean hydrodynamical diameter (D_H) from NTA plotted in function of the solute mass fraction (Φ) normalized by the corresponding mass fractions at the cloudiness curve (Φ**); and phase diagrams build through visual observation (light grey= limpid; dark grey = diphasic; hatched= cloudy).*

Investigation of water/THF/BODIPY: case of a solid fluorescent solute. Until now, most studies on the Ouzo effect have dealt with either oils or polymers which leave little doubt about the physical state of the dispersed phase (i.e. liquid for oils and solid for polymers). One noticeable exception is the case of the system water/ethanol/anethol (model system for the Ouzo or Pastis beverages), the melting point of anethol being around 21°C [2,15]. The BHT is another example of low molecular weight solid solute. In these cases, the physical state of the particles depends on their composition. Indeed, the phases of a separated ternary system can contain different amounts of the three constituents. It is generally assumed that in the case of Ouzo emulsions the droplets consist mostly of solute, but they may be more or less swollen with the solvent and even contain traces of water. The most rigorous method to determine the composition of the phases in equilibrium is to build the tie lines in the phase diagram [20]. However, this method is not applicable when one of the compounds is at extremely low concentration, as it is the case here. The above results concerning the NMR study of the water/THF/BHT system show that the dispersed phase in the Ouzo domain can remain liquid. Here, we took advantage of a fluorescent dye, that is emissive in the liquid and the solid states with

different wavelengthes, to investigate the physical state of a solid solute through the phase diagram. We used a home made BODIPY dye (Figure 5) that yields a strong green emission when solubilized in organic solvents and a weaker red emission in the solid state (Figure SI-9) [10]. We investigated the water/THF/BODIPY system. In contrast to previous systems, it was not possible to determine the cloudiness curve because of the fluorescence of BODIPY. Instead, we displayed the color of the samples under UV illumination in a "diagram of emission" (Figure 5). Very dilute samples ($\Phi_{BODIPY} < 10^{-6}$) look dark because they emit weakly. As expected, green emission is more intense in the solvent rich region (up-left part of the diagram). When increasing the amount of dye, the green emission decreases at the benefit of the red emission, indicating the presence of solid BODIPY particles. We used SLMS stability analysis (Figure SI-10) along the composition lines Φ_{THF}=0.1, 0.2, 0.3 and 0.4 to build the binodal curve. Note that the SMLS uses a NIR laser at 880 m, which is far away from the excitation range of the BODIPY. For each line, we determined the boundary between stable and evolving samples. As previously, this draws a linear curve that we superimposed on the emission diagram in the Figure 5. Most samples along the binodal curve emit green light. We centrifugated two samples beyond the binodal, presenting yellow (f_1: Φ_{THF}=0.2; Φ_{BODIPY}=2.5 10^{-5}) and red (f_2: Φ_{THF}=0.2; Φ_{BODIPY}=2.5 10^{-4}) emission. Very interestingly, their pellets emit yellow and red light under irradiation for samples f_1 and f_2 respectively (Figure 5), indicating that the composition of the dispersed phase evolves from BODIPY swollen with solvent to pure solid BODIPY.

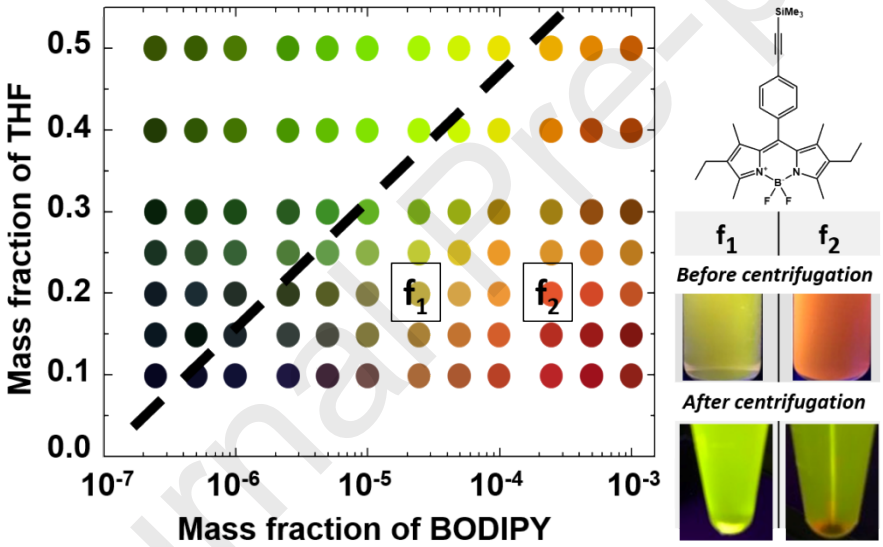

Figure 5: Chemical structure of the BODIPY dye and diagram of fluorescence emission (λ_{exc} =365 nm). The dashed line is the limit between stable and evolving samples as determined by SMLS. f_1 and f_2 represent the compositions that were centrifugated (f_1: Φ_{THF}=0.2; Φ_{BODIPY}=2.5 10^{-5} ; f_2: Φ_{THF}=0.2; Φ_{BODIPY}=2.5 10^{-4}).

NTA analysis proved to be limited to very dilute samples due to the excitation of BODIPY fluorescence at the operating wavelength (405 nm), but DLS measurements with laser wavelength of 638 nm could be achieved. Therefore, we monitored the samples for 3 hours after preparation using DLS. The results for the composition line Φ_{THF}= 0.2 are displayed in Figure 6a. The first observation is that there exists a SFME domain in the range (Φ_{BODIPY} = 10^{-7}- 2.5 10^{-6}), with stable droplets of diameter ca 100 nm,

that remain stable in time. At larger concentrations (5.10^{-6} and beyond), the size evolves with time. These observations are consistent with the SMLS measurements and confirm the location of the binodal curve.
Finally, we measured the electrophoretic mobility of samples along the dilution line Φ_{THF}=0.2 (Figure 6b) using an instrument operating at 633 nm. As previously, we find a maximum of (negative) mobility at the binodal, related to a strongly negative charge at the interface. As previously, the evolution of electrophoretic mobility is consistent with that the colloidal stability as observed with the DLS and SMLS analysis.

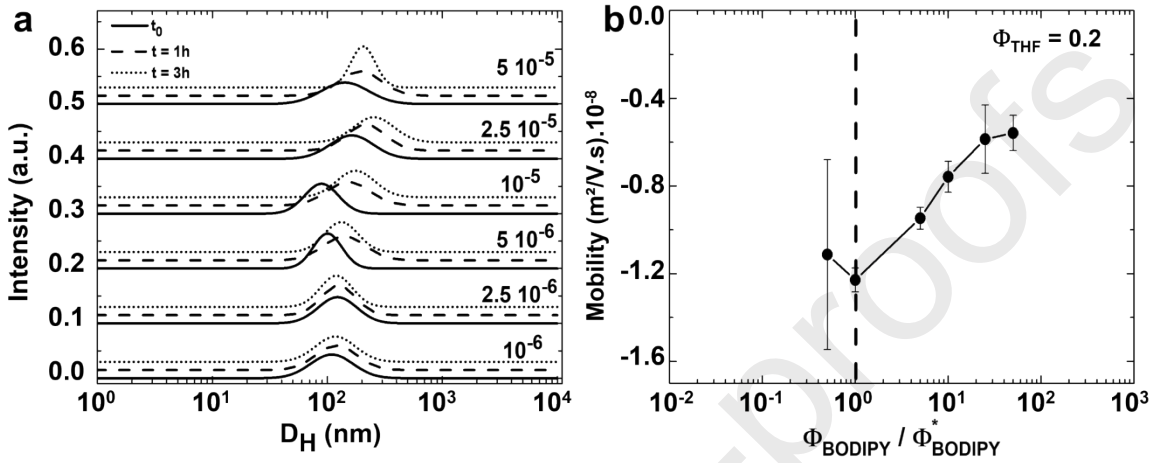

Figure 6: Investigation of the composition line Φ_{THF} = 0.2 of the system water/THF/BODIPY (a) DLS measurements at initial time (──); after 1 h (- - -); after 3 h (·····). (b) Electrophoretic mobility of the dispersed phase in function of the mass fraction of BODIPY normalized by the fraction at the binodal.

4.Conclusion

As an attempt to clarify the general behavior of Ouzo emulsions and the methodology to determine unambiguously the binodal curve, we achieved a careful examination of four ternary systems, with low molecular weight solutes, both liquid and solids. In contrast to many other studies, we did not make use of surfactant to avoid any interference with the pristine systems. We hypothesized that combining conventional DLS analysis with stability monitoring would allow us to delineate the Ouzo domain. This assumption is not obvious, as homogeneous supersaturated states can exist in a metastable zone. However, in the case of the Ouzo effect, nucleation is initiated since by definition particles are present. It is the growth of the droplets that is kinetically blocked or slowed down [15]. Thus, stability studies using SMLS, but also NTA or DLS, have allowed us to effectively discriminate Ouzo domain aggregates (more or less slowly evolving) from SFME aggregates (thermodynamically stable), validating this original approach.
In most studies to date, phase diagrams have been constructed on the basis of visual observation of cloudiness and/or size analysis by scanning electron microscopy (SEM), DLS or other size analysis techniques [1,9,41,42]. In addition, surfactants can be added to the system to ensure colloidal stability of the particles during the analysis time [9,43]. Consequently, the criteria for defining the Ouzo domain have been variable. Thus, the boundary between the monophasic and the Ouzo domains is often taken by construction as the onset of cloudiness, determined by visual observation. In other cases, the measurement of the mean hydrodynamic radius was used as a criterion [9,16]. Indeed, the evolution of this diameter with the solute concentration shows two regimes: a constant regime and a regime where the size increases with the solute concentration. The transition between these two regimes has been interpreted as the boundary between SFME and Ouzo. Note that several works are based on the assumption that an Ouzo system should

be cloudy and do not provide an analysis of the transparent zone [1,44]. Regarding the high-concentration boundary of the Ouzo domain, SEM-based studies (mostly in the case of polymers) have used a size-dispersity criterion, to define the "stable" *vs* "unstable" Ouzo domains [13,42]. In some other cases, compositions that were cloudy but not demixed after a "certain time" were considered as Ouzo emulsions [28].

While we have addressed the case of low molecular weight solute (solid or liquid), many other studies have focused on nanoprecipitation of polymers by solvent-shifting. Significant differences can be noted. Indeed, in the case of polymers, the solubility limit is not very dependent on the polymer concentration, which would be reflected by an almost horizontal line in the representation of figure 1a [13,42]. Moreover, detailed studies of the dependence of particle size with solvent and/or polymer concentration showed that polymer particles form by a nucleation-aggregation mechanism, favoring a narrow size distribution [13]. In fact, the surface area of the domain where particles with a low size distribution are observed is generally much larger than with low molecular weight compounds. It is our opinion that in the case of polymers, nucleation-growth readily yields particles of homogeneous size (which are termed "stable Ouzo"), and that polydisperse compositions containing micron-sized particles (termed "unstable Ouzo") appear in the vicinity of the spinodal. It should also be noted that surfactants are commonly used to limit the aggregation of polymer particles and can influence the nucleation conditions, in particular by reducing the critical radius of nucleation [5,41].

The control of the physical state of nanoprecipitates (liquid, amorphous solid or crystalline) is very important, as it governs the solubility and therapeutic properties of certain drugs. Although most studies show that nanoprecipitation rarely leads to a crystalline structure, the reasons for this are still debated [5]. One hypothesis is the presence of solvent, acting as a plasticizer of the particles, but experimental evidence is lacking. The SANS technique, particularly with contrast variation, could be used in combination with models to determine the composition and structure (homogeneous, core-shell) of the droplets/particles at moderate dilutions [25,30]. Thus, one previous SANS study suggested that the aggregates formed in the SFME domain of the D_2O/THF/BHT system consist of a small BHT core surrounded by a large THF shell [30]. Nevertheless, our NMR and fluorescence measurements here clearly established the presence of solvent with the solute in the dispersed phase. Note that the few previous NMR studies of the Ouzo effect, were carried out on liquid solutes at 25°C (anethole or toluene) and aimed to characterize the exchange dynamics between the dispersed and continuous phases [28,35].

The metastability of the droplets is one of the most intriguing features of the Ouzo emulsions. While droplet coalescence rate decreases with concentration, the generally high dilution of Ouzo domain is not enough to explain their stability, some times over months [15]. The adsorption of charged species at the interface has been proposed as an alternative explanation, and experimental evidences of the existence of a negative surface charge on emulsions produced by solvent-shifting were provided [18,39,45]. This surface charge obviously has a pH signature and appears to be due either to the direct adsorption of endogenous CO_3^{2-}, HCO^{3-} or OH^- ions at the interface or to the reaction of hydroxyl ions with acidic impurities. Here, for the first time, we follow the evolution of the charge with hydrophobic solute composition, from the SFME domain to the Ouzo domain, and show a regime change at the binodal, which can be related to a change in the composition of the dispersed objects.

In summary, the combination of conventional (DLS, Nanoparticle Tracking Analysis or NTA) and less conventional (NMR, stability analysis by SMLS, zeta potential, fluorescence) techniques allowed us to challenge conventional views on spontaneous emulsifications. We show that all four systems exhibit a SFME domain, separated from the Ouzo domain by the binodal curve. There is no discontinuity of size at

the binodal but this transition can be determined by monitoring the colloidal stability of the sample. In addition, the droplets bear a spontaneous negative charge that shows a maximum at the binodal. Importantly, we clearly evidence that Ouzo emulsions can be transparent, and that the finest emulsions are generated in the transparent domain in between the binodal and the cloudiness curves. The cloudiness curve marks the abrupt increase in polydispersity. These results call into question the method of visual observation to identify the Ouzo domain, widely used in nanoprecipitation processes, and can be used as a rational guide for the design of nanoparticles and nanocapsules with polymers, drugs, or inorganic materials.

There is still much to be understood about the transition between the SFME and Ouzo domains. We believe that future works should focus on analyzing both the composition and the structure of the dispersed phase in both domains. Short times kinetic experiments (using stopped-flow devices) may also provide interesting views on the early moments of droplet nucleation.

Acknowledgment: We wish to thank the region Bretagne (ARED-107/ NAPOLI), the ANR (grant: 2020-CES06-OuzoFan), the CNRS, the University Rennes 1 and the platform ScanMat (2Cbiomif) for funding. Part of this work has been performed using the PRISM core facility (Biogenouest, Univ Rennes, Univ Angers, INRAE, CNRS, FRANCE): the authors thank Sandrine Pottier and Dr. Arnaud Bondon for their precious help and expertise. We very warmly thank Olivier Mongin for providing the BODIPY and Anthony Szymczyk and Bertrand Lefeuvre for complimentary access to the DLS.

[1] S.A. Vitale, J.L. Katz, Liquid Droplet Dispersions Formed by Homogeneous Liquid−Liquid Nucleation: “The Ouzo Effect,” Langmuir. 19 (2003) 4105
[2] I. Grillo, Small-angle neutron scattering study of a world-wide known emulsion: Le Pastis, Colloids and Surfaces A: Physicochemical and Engineering Aspects. 225 (2003) 153
[3] L. Chiappisi, I. Grillo, Looking into Limoncello: The Structure of the Italian Liquor Revealed by Small-Angle Neutron Scattering, ACS Omega. 3 (2018) 15407
[4] E. Scholten, E. van der Linden, H. This, The Life of an Anise-Flavored Alcoholic Beverage: Does Its Stability Cloud or Confirm Theory?, Langmuir. 24 (2008) 1701
[5] E. Lepeltier, C. Bourgaux, P. Couvreur, Nanoprecipitation and the “Ouzo effect”: Application to drug delivery devices, Advanced Drug Delivery Reviews. 71 (2014) 86
[6] C.J. Martínez Rivas, M. Tarhini, W. Badri, K. Miladi, H. Greige-Gerges, Q.A. Nazari, S.A. Galindo Rodríguez, R.Á. Román, H. Fessi, A. Elaissari, Nanoprecipitation process: From encapsulation to drug delivery, International Journal of Pharmaceutics. 532 (2017) 66
[7] F. Ganachaud, J.L. Katz, Nanoparticles and Nanocapsules Created Using the Ouzo Effect: Spontaneous Emulsification as an Alternative to Ultrasonic and High-Shear Devices, ChemPhysChem. 6 (2005) 209
[8] X. Yan, M. Delgado, A. Fu, P. Alcouffe, Sø.G. Gouin, E. Fleury, J.L. Katz, F. Ganachaud, J. Bernard, Simple but Precise Engineering of Functional Nanocapsules through Nanoprecipitation, Angew. Chem. (2014) 7030
[9] X. Yan, P. Alcouffe, G. Sudre, L. David, J. Bernard, F. Ganachaud, Modular construction of single-component polymer nanocapsules through a one-step surfactant-free microemulsion templated synthesis, Chemical Communications. 53 (2017) 1401–1404. https://doi.org/10.1039/C6CC09701D.

[10] C. Goubault, F. Sciortino, O. Mongin, U. Jarry, M. Bostoen, H. Jakobczyk, A. Burel, S. Dutertre, M.-B. Troadec, M.L. Kahn, S. Chevance, F. Gauffre, The Ouzo effect: A tool to elaborate high-payload nanocapsules, Journal of Controlled Release. 10 (2020) 430
[11] C. Goubault, U. Jarry, M. Bostoën, P.-A. Éliat, M.L. Kahn, R. Pedeux, T. Guillaudeux, F. Gauffre, S. Chevance, Radiosensitizing Fe-Au nanocapsules (hybridosomes®) increase survival of GL261 brain tumor-bearing mice treated by radiotherapy, Nanomedicine: Nanotechnology, Biology and Medicine. 40 (2022) 102499.
[12] C. Pucci, F. Cousin, F. Dole, J.-P. Chapel, C. Schatz, Impact of the Formulation Pathway on the Colloidal State and Crystallinity of Poly-ε-caprolactone Particles Prepared by Solvent Displacement, Langmuir. 34 (2018) 2531
[13] J. Aubry, F. Ganachaud, J.-P. Cohen Addad, B. Cabane, Nanoprecipitation of Polymethylmethacrylate by Solvent Shifting:1. Boundaries, Langmuir. 25 (2009) 1970
[14] R. Botet, K. Roger, How do interactions control droplet size during nanoprecipitation?, Current Opinion in Colloid & Interface Science. 22 (2016) 108
[15] N.L. Sitnikova, R. Sprik, G. Wegdam, E. Eiser, Spontaneously Formed *trans* -Anethol/Water/Alcohol Emulsions: Mechanism of Formation and Stability, Langmuir. 21 (2005) 7083
[16] C. Goubault, D. Iglicki, R.A. Swain, B.F.P. McVey, B. Lefeuvre, L. Rault, C. Nayral, F. Delpech, M.L. Kahn, S. Chevance, F. Gauffre, Effect of nanoparticles on spontaneous Ouzo emulsification, Journal of Colloid and Interface Science. 603 (2021) 572
[17] K. Roger, R. Botet, B. Cabane, Coalescence of Repelling Colloidal Droplets: A Route to Monodisperse Populations, Langmuir. 29 (2013) 5689
[18] F. Ganachaud, X. Yan, M. Delgado, J. Aubry, O. Gribelin, A. Stocco, F. Boisson-Da Cruz, J. Bernard, Central Role of Bicarbonate Anions in Charging Water/Hydrophobic Interfaces, J. Phys. Chem. Lett. 9 (2018) 96
[19] K. Roger, M. Eissa, A. Elaissari, B. Cabane, Surface Charge of Polymer Particles in Water: The Role of Ionic End-Groups, Langmuir. 29 (2013) 11244
[20] A. Arce, A. Arce, O. Rodriguez, Revising Concepts on Liquid–Liquid Extraction: Data Treatment and Data Reliability, J. Chem. Eng. Data. 67 (2022) 286
[21] M.L. Klossek, D. Touraud, W. Kunz, Eco-solvents – cluster-formation, surfactantless microemulsions and facilitated hydrotropy, Phys. Chem. Chem. Phys. 15 (2013) 10971
[22] W. Hou, J. Xu, Surfactant-free microemulsions, Current Opinion in Colloid & Interface Science. 25 (2016) 67
[23] A. Lucia, P.G. Argudo, E. Guzmán, R.G. Rubio, F. Ortega, Formation of surfactant free microemulsions in the ternary system water/eugenol/ethanol, Colloids and Surfaces A: Physicochemical and Engineering Aspects. 521 (2017) 133
[24] T.N. Zemb, M. Klossek, T. Lopian, J. Marcus, S. Schöettl, D. Horinek, S.F. Prevost, D. Touraud, O. Diat, S. Marčelja, W. Kunz, How to explain microemulsions formed by solvent mixtures without conventional surfactants, Proc Natl Acad Sci USA. 113 (2016) 4260
[25] S. Prévost, S. Krickl, S. Marčelja, W. Kunz, T. Zemb, I. Grillo, Spontaneous Ouzo Emulsions Coexist with Pre-Ouzo Ultraflexible Microemulsions, Langmuir. 37 (2021) 3817
[26] O. Diat, M.L. Klossek, D. Touraud, B. Deme, I. Grillo, W. Kunz, T. Zemb, Octanol-rich and water-rich domains in dynamic equilibrium in the pre-ouzo region of ternary systems containing a hydrotrope, J Appl Crystallogr. 46 (2013) 1665
[27] D.M. Bassani, D. Carteau, I. Pianet, P. Brunerie, B. Guillemat, Probing the Initial Events in the Spontaneous Emulsification of *trans* -Anethole Using Dynamic NMR Spectroscopy, Langmuir. 23 (2007) 3561
[28] A.R. Tehrani-Bagha, A. Viladot, K. Holmberg, L. Nordstierna, An Ouzo emulsion of toluene in water characterized by NMR diffusometry and static multiple light scattering, Colloids and Surfaces A: Physicochemical and Engineering Aspects. 494 (2016) 81

[29] F. Sciortino, G. Casterou, P.-A. Eliat, M.-B. Troadec, C. Gaillard, S. Chevance, M.L. Kahn, F. Gauffre, Simple Engineering of Polymer-Nanoparticle Hybrid Nanocapsules, ChemNanoMat. 2 (2016) 796
[30] Z. Li, H. Cheng, J. Li, J. Hao, L. Zhang, B. Hammouda, C.C. Han, Large-Scale Structures in Tetrahydrofuran–Water Mixture with a Trace Amount of Antioxidant Butylhydroxytoluene (BHT), J. Phys. Chem. B. 115 (2011) 7887
[31] N.F. Bunkin, A.V. Shkirin, G.A. Lyakhov, A.V. Kobelev, N.V. Penkov, S.V. Ugraitskaya, E.E. Fesenko, Droplet-like heterogeneity of aqueous tetrahydrofuran solutions at the submicrometer scale, The Journal of Chemical Physics. 145 (2016) 184501
[32] G. Ulrich, R. Ziessel, Convenient and Efficient Synthesis of Functionalized Oligopyridine Ligands Bearing Accessory Pyrromethene-BF_2 Fluorophores. J. Org. Chem. 69, (2004) 2070
[33] N.R. Mahendra, B. Das, D.K. Hazra, Densities and viscosities of the binary aqueous mixtures of tetrahydrofuran and 1,2-dimethoxyethane at 298, 308 and 318 K, Indian J. Chem. Technol. (1994) 5
[34] J. Jeener, B.H. Meier, P. Bachmann, R.R. Ernst, Investigation of exchange processes by two-dimensional NMR spectroscopy, J. Chem. Phys. 71 (1979) 4546
[35] D. Carteau, D. Bassani, I. Pianet, The "Ouzo effect": Following the spontaneous emulsification of trans-anethole in water by NMR, Comptes Rendus Chimie. 11 (2008) 493
[36] R. Kaiser, Use of the Nuclear Overhauser Effect in the Analysis of High-Resolution Nuclear Magnetic Resonance Spectra, J. Chem. Phys. 39 (1963) 2435
[37] F.A.L. Anet, A.J.R. Bourn, Nuclear Magnetic Resonance Spectral Assignments from Nuclear Overhauser Effects1, J. Am. Chem. Soc. 87 (1965) 5250
[38] M. Frunzi, A.M. Baldwin, N. Shibata, S.-I. Iwamatsu, R.G. Lawler, N.J. Turro, Kinetics and Solvent-Dependent Thermodynamics of Water Capture by a Fullerene-Based Hydrophobic Nanocavity, J. Phys. Chem. A. 115 (2011) 735
[39] K. Roger, B. Cabane, Why Are Hydrophobic/Water Interfaces Negatively Charged?, Angewandte Chemie International Edition. 51 (2012) 5625
[40] R. Vácha, S.W. Rick, P. Jungwirth, A.G.F. de Beer, H.B. de Aguiar, J.-S. Samson, S. Roke, The Orientation and Charge of Water at the Hydrophobic Oil Droplet–Water Interface, J. Am. Chem. Soc. 133 (2011) 10204
[41] M. Beck-Broichsitter, J. Nicolas, P. Couvreur, Solvent selection causes remarkable shifts of the "Ouzo region" for poly(lactide-co-glycolide) nanoparticles prepared by nanoprecipitation, Nanoscale. 7 (2015) 9215
[42] J.-P. Chapel, C. Pucci, F. Cousin, F. Dole, C. Schatz, Impact of the Formulation Pathway on the Colloidal State and Crystallinity of Poly-ε-caprolactone Particles Prepared by Solvent Displacement, Langmuir. 34 (2018) 2531
[43] J. Marcus, D. Touraud, S. Prévost, O. Diat, T. Zemb, W. Kunz, Influence of additives on the structure of surfactant-free microemulsions, Phys. Chem. Chem. Phys. 17 (2015) 32528
[44] M. Beck-Broichsitter, E. Rytting, T. Lebhardt, X. Wang, T. Kissel, Preparation of nanoparticles by solvent displacement for drug delivery: A shift in the "ouzo region" upon drug loading, European Journal of Pharmaceutical Sciences. 41 (2010) 244
[45] A. Ma, J. Xu, H. Xu, Impact of Spontaneously Adsorbed Hydroxide Ions on Emulsification via Solvent Shifting, J. Phys. Chem. C. 118 (2014) 23175

Graphical abstract

Shedding Light on the Formation and Stability of Mesostructures in Ternary "Ouzo" Mixtures

Déborah Iglicki, Clément Goubault, Mouktar Nour Mahamoud, Soizic Chevance and Fabienne Gauffre

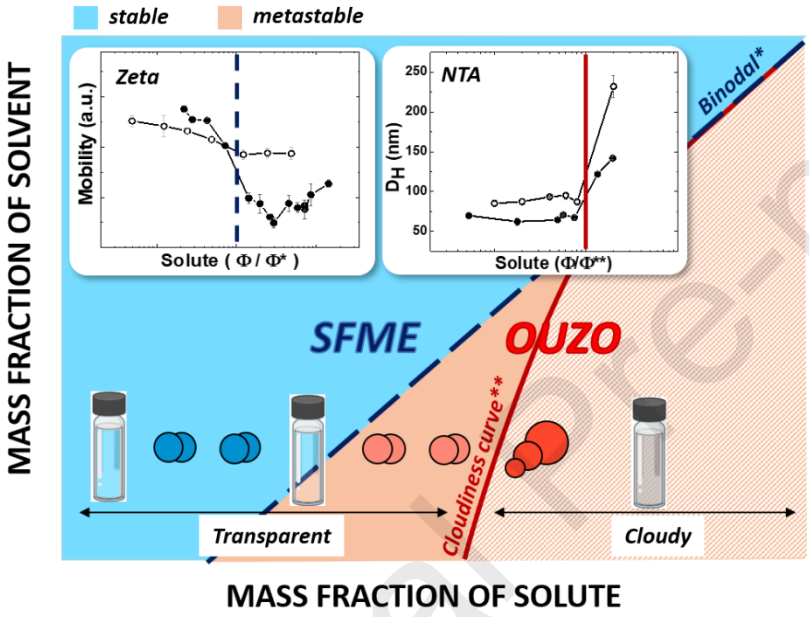

Credit author Statement

Déborah Iglicki: Conceptualization ; Investigation ; Visualization; Review and Editing

Clément Goubault: Conceptualization ; Investigation ; Review and Editing

Mouktar Nour: Investigation

Soizic Chevance: Conceptualization ; Investigation ; Writing - Original Draft ; Review and Editing; Supervision

Fabienne Gauffre: Conceptualization ; Writing - Original Draft ; Review and Editing ; Funding acquisition ; Supervision

Declaration of interests

☒ The authors declare that they have no known competing financial interests or personal relationships that could have appeared to influence the work reported in this paper.

☐ The authors declare the following financial interests/personal relationships which may be considered as potential competing interests: